A General Framework and Optimization for Spatially-Coupled Serially Concatenated Systems

Tarik Benaddi
Lab-STICC/IMT Atlantique
tarik.benaddi@imt-atlantique.fr

Charly Poulliat
IRIT/INPT-ENSEEIHT
charly.poulliat@enseeiht.fr

Romain Tajan
IMS/Bordeaux INP-ENSEIRB
romain.tajan@ims-bordeaux.fr

***Abstract*—In this paper, we provide a general framework for spatially-coupled concatenated systems. We explicit the analogy with spatially-coupled protographs and provide an adapted EXIT chart analysis. By proposing a continuous-valued coupling matrix, we propose a code design procedure for faster convergence. When considering general bit-interleaved coded-modulation scheme, we also conjecture that the spatially-coupled scheme of general detectors saturates to a value very close (lower bound) to the threshold given by the Area theorem.**

***Index Terms*—Turbo codes, Spatially coupling, AWGN, EXIT charts, Saturation, bit-interleaved coded-modulation, Faster-than-Nyquist**

I. Introduction

The convolutional counterparts of LDPC codes are called LDPC convolutional (LDPC-C) codes [1]. They are obtained by spatial coupling of LDPC codes and can also be described by a sparse parity check matrix and consequently being decoded with message passing decoding algorithms. Because of the coupling, this family of codes show very good thresholds thanks to the so-called saturation phenomenon: it was proven for the Binary Erasure Channel (BEC) that the threshold under belief propagation decoding converges to the optimal Maximum *a posteriori* (MAP) threshold [2]. Later on, an other proof using the potential function extended these results to other channels [3], [4]. Different methods can be used to construct LDPC-C such as unwrapped LDPC codes [5] or spatially-coupled protograph codes [6].

Recently, different papers extended the spatial coupling to serial and parallel concatenated turbo-codes [7]–[10] and derived the saturation proof for the BEC channel. In [7], [8], authors proposed the spatial coupling of systematic parallel and serial turbo-codes and concluded that for the BEC, coupled serially concatenated schemes have better threshold than their parallel counterparts. In order to terminate the spatially coupled ensemble, they proposed to force the last information symbols to zeros. Finally, they studied rate compatible ensembles using puncturing.

In [11], same authors studied the finite length performance of braided convolutional codes (BCC) and showed that the minimum distance of the coupled ensemble is lower bounded by the the minimum distance of the uncoupled ensemble. In [9], the authors reviewed the literature results on BCC and present an unified description on BCC with respect to other turbo-like codes.

In this paper, we intend to generalize previous works to the framework of the spatial coupling of general serially concatenated systems. First, we will describe the proposed coupling procedure, then we show that it is actually the spatial coupling of a generalized multi-edge type (MET) or protograph LDPC code [12]. Secondly, inspired by Protograph EXIT (P-EXIT) charts [13], we describe the EXIT chart equations to study the asymptotic behaviour of such systems. We also explain where the coupling gain comes from and describe the termination and the tail-biting procedures. Thirdly, thanks to the proposed framework, we explore the effect of the syndrome former memory and, by redefining the proposed coupling matrix into a continuous-valued matrix, we introduce an optimization procedure that optimizes the coupling in order to reduce the number of iterations before convergence. Finally, we discuss some results and we conjecture that the threshold of spatially-coupled serially concatenated systems is lower bounded by the threshold given by the area theorem [14].

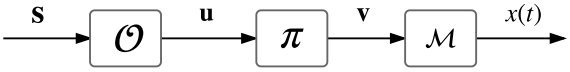

Fig. 1: The transmitter

II. System description

Without loss of generality, as an example of serially concatenated system, we consider in this paper general bit-interleaved coded-modulation (BICM) schemes where the outer component is an error correcting code and the inner component is a general modulation scheme (coded modulation or modulation with memory as in the case of faster-than-Nyquist scheme).

A. General spatially coupled Bit-interleaved coded modulation schemes

Let us consider the serially concatenated scheme composed of an error correcting code and a modulator as depicted in Fig. 1. For ease of exposition, we consider the simple case of a convolutional code. First, a k-bits information block $\boldsymbol{s} \in \{0,1\}^k$ is encoded with the outer code, denoted $\mathcal{O}$, into a n-bits coded block $\boldsymbol{u} \in \{0,1\}^n$ (the code rate is $R = k/n$). Then, the sequence $\boldsymbol{u}$ is interleaved by the an interleaver π to obtain $\boldsymbol{v}$ and mapped into $\boldsymbol{x} = \{x_i\}_i$ with $x_i \in \{0, \dots, M-1\}$ where M is the modulation order. Finally, the vector $\boldsymbol{x}$ is modulated into the analog signal $x(t)$ using a shaping filter. For ease of notations, the mapping and the shaping are considered jointly and constitute the modulator $\mathcal{M}$.

In this paper, we assume that the complex signal $x(t)$ is sent over an additive white Gaussian noise (AWGN) channel with a one-sided power spectral density N_0.

At the receiver side, a classical iterative turbo receiver is considered [15], [16]: the received signal $y(t)$ is first

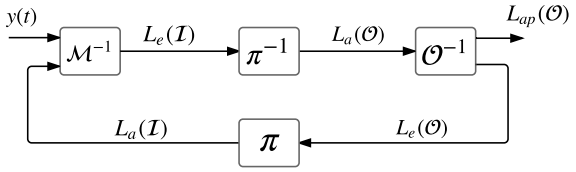

Fig. 2: The receiver

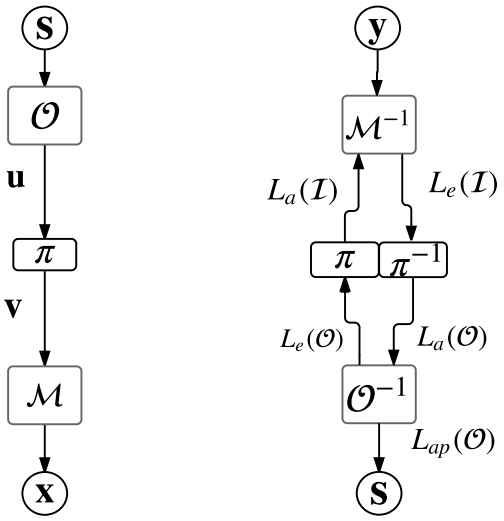

Fig. 3: The compact graph of the encoder (left) and the decoder (right)

processed by a soft-input soft-output (SISO) demodulator $\mathcal{M}^{-1}$. The obtained extrinsic log-likelihood ratios (LLRs) of the demodulated bits, $L_e(\mathcal{I})$, are deinterleaved and used as an *a priori* LLRs, $L_a(\mathcal{O})$, by the outer decoder $\mathcal{O}^{-1}$. This latter runs a BCJR algorithm [17] and provides the extrinsic LLRs corresponding to the coded bits, $L_e(\mathcal{O})$. When interleaved, these latter constitute the *a priori* LLRs of the demodulated bits, denoted $L_a(\mathcal{I})$ of the SISO $\mathcal{M}^{-1}$. After a fixed number of turbo iterations, the estimated information bits are deduced from the sign of the *a posteriori* LLRs of the decoded bits $L_{ap}(\mathcal{O})$. A sketch of the turbo receiver architecture with the exchanged LLR messages is depicted in Fig. 2.

Inspired by the representation of multi-edge type (MET) LDPC codes and protograph codes [12], we propose the vectorized view of Figs. 1 and 2 depicted in Fig. 3. The information and the transmitted bits sequences $\boldsymbol{s}$ and $\boldsymbol{x}$ are represented by circular nodes, the inner and the outer components are represented by rectangles and the interleavers are placed above the corresponding edges. By a slight abuse of notation, the estimated information bits are also denoted by $\boldsymbol{s}$. A very similar representation was proposed by [7], [9] and was referred to as *the compact graph representation*. We will adopt the same terminology.

B. Spatially-Coupled BICM

In this section, we describe how one can spatially couple the concatenated scheme in Fig. 3. Our proposed framework is in spirit equivalent to [7]–[10], [18], however, its formalism provides better control on design tools (component base matrix, coupling procedure, mapping optimisation, termination) and presents analogous properties to those of spatially-coupled protograph codes [6] (rate loss, component base matrix, two coupling "waves", tail-biting ...).

Inspired from spatially-coupled protographs, spatially-coupled turbo-codes (SC-TC) can be obtained by a variant of the edge spreading rule (ESR) [6]: in the compact graph, the encoded bits $\boldsymbol{v}$ are demultiplexed into m_s+1 bundles, and the obtained graph is replicated a certain number of times, say L. Afterwards, the L graphs are interconnected by interchanging the ends of the bundles of the same type. In order to describe these interconnections, we introduce the integer-valued coupling matrix B defined as:

$$B = [b_0, b_1, \dots b_{m_s}] \in \{0, \dots n\}^{m_s+1}$$

where b_i represents the width (number of bits) of the bundle connecting any copy t with its adjacent neighbour $(t+i)$. B should verify $\sum_{i=0}^{m_s} b_i = n$.

Alike spatially-coupled LDPC codes, L is called the coupling length and m_s the syndrome former memory. For code design and convergence analysis purposes, as we are going to see later, it is more convenient to consider a continuous-valued coupling matrix. To this end, we will rather divide B by n: now, $b_i \in [0, 1]$ is interpreted as the fraction of the bits $\boldsymbol{u}$ passed from the constituent code of the stage t to the stage $(t+i)$. We then have:

$$\sum_{i=0}^{m_s} b_i = 1 \tag{1}$$

An example of this construction is illustrated in Fig. 4.

C. Tail-biting

In the coupled compact graph, one can notice that we end up with some vacant bundles connections at the beginning and some additional unconnected bundles at the end. One way to solve this problem is by connecting these latter all the way back with the former. This is called tail-biting and one can easily show that the rate of the obtained SC-TC is exactly equal to R. However, this scheme does not show the desired coupling gain since, locally, each stage behaves exactly as the underlying TC scheme in Fig. 3.

D. Termination

A second solution is:

- adding m_s modulators at the end in order to connect the last remaining bundles
- adding known information bits at the m_s first and the m_s last mappers in order to fill the vacant bundles connections

A simple example is depicted in Fig. 5. The m_s black circles at the boundaries represent the added known bits.

We can show that, in this case, the final code rate of the coupled ensemble, when puncturing is not used, is equal to:

$$R_L = \frac{L}{L+m_s} R = R - \frac{m_s}{L+m_s} R \tag{2}$$

which is analogous to the design rate of spatially-coupled protographs. Observe that the termination (finite value of L) results in a rate loss equal to $\frac{m_s}{L+m_s} R$. This penalty vanishes to 0 as $L \to +\infty$.

The difference of Eq. (2) with the rate expression computed in [8] comes from the following reasons:

- Their rate loss is induced by last imposed $'0's$ information bits used to terminate the encoder to the

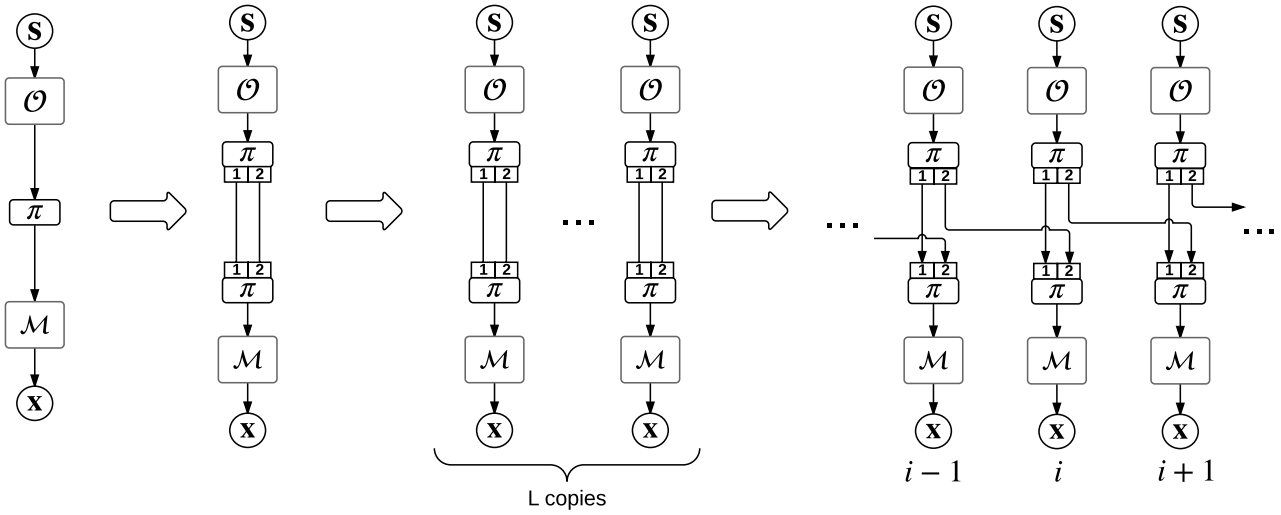

Fig. 4: SC TC transmitter. The coupling is done according to $B = [0.5, 0.5]$.

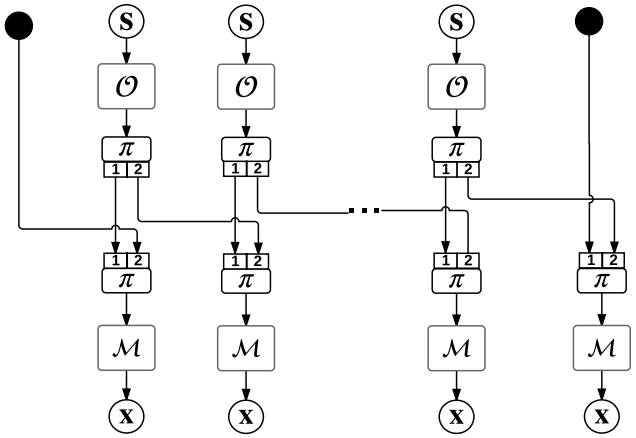

Fig. 5: Terminated spatially-coupled turbo-codes

zero state[1]. In our case, the rate loss is caused by the additional ending mappers and by the inserted known bits at the boundaries (to keep a constant number of output bits $\boldsymbol{x}$ at all stages).

- Eq. (2) stands for both systematic and non systematic codes

As it is going to be showed later, the less connected mappers[2] (alike the less connected check nodes at the boundaries of spatially-coupled protographs) induce a *wave effect* phenomenon: the known bits at the boundaries will help generating more reliable LLRs, which, through iterations, will progressively propagate towards the center. The intermediate stages will behave the same way as the uncoupled system, as far as the coupling gain did not affect them yet.

III. Asymptotic Convergence Analysis

In this section, we perform the asymptotic convergence analysis of the SC-TC. Density evolution (DE) was considered in [18] to analyze the performance over the binary erasure channel (BEC). In the case of AWGN and with general inner and outer components, evaluating the threshold by tracking the evolution of the density of the messages become a prohibitive task. Alternatively, EXIT charts [19] are usually considered.

A. Exit Chart of the uncoupled system

For a fixed channel parameter, here the symbol (or bit) energy to noise ratio E_s/N_0 (resp. E_b/N_0), the EXIT charts track the evolution of the mutual information (MI) between the current extrinsic LLRs and the corresponding bits through iterations. To this end, it uses the input-output transfer function of the different SISO blocks (here the SISO of the inner and the SISO of the outer components). As depicted in Fig. 3, the demodulator transfer function $T_{\mathcal{M}}(.)$[3] computes the extrinsic MI $I_e(\mathcal{I})$ (between the LLRs $L_e(\mathcal{I})$ and the corresponding bits) based on the channel observations and the *a priori* MI $I_a(\mathcal{I})$ (between $L_a(\mathcal{I})$ and the corresponding bits). Similarly, the outer decoder transfer function $T_{\mathcal{O}}(.)$ computes both the extrinsic MI $I_e(\mathcal{O})$ (between $L_e(\mathcal{O})$ and the corresponding bits) and the *a posteriori* MI $I_{ap}(\mathcal{O})$(between the LLRs $L_{ap}(\mathcal{O})$ of the corresponding bits) based on the *a priori* MI $I_a(\mathcal{O})$ (of $L_a(\mathcal{O})$ and the corresponding bits).

We perform the demodulator and the outer decoder updates until the maximum number of iterations is reached (no convergence) or $I_{ap}(\mathcal{O}) = 1, \forall i$ (convergence). The analytic expressions of $T_{\mathcal{O}}(.)$ and $T_{\mathcal{M}}(.)$ are not available in the general case, consequently, we estimated them by Monte Carlo simulations. An example of EXIT charts and corresponding recursions steps are depicted in [14, Fig. 6].

B. Spatially-coupled EXIT (SC-EXIT) chart

For our analysis, we consider the i^{th} stage of the spatially-coupled compact graph depicted in Fig. 6. The following notations are used:

- The subscript i differentiate between variables relative to each stage;
- $I_e^k(i^+)$ (resp. $I_a^k(i^+)$) is the extrinsic (resp. *a priori*) MI between the LLRs transmitted from $\mathcal{M}_i^{-1}$ (resp. from $\mathcal{O}_{i+k}^{-1}$) to $\mathcal{O}_{i+k}^{-1}$ (resp. to $\mathcal{M}_i^{-1}$);

[1]The "zero state" refers to the overall SC scheme (*i.e.* last transmitted symbol are 0's) and not the internal state of each constituent code

[2]*less connected* because they have lesser real information bits at their inputs in comparison to their counterparts

[3]$T_{\mathcal{M}}(.)$ depends implicitly on E_b/N_0

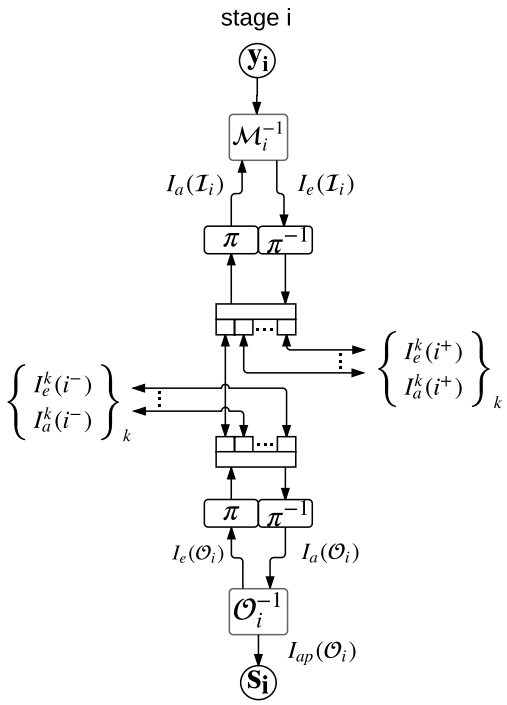

Fig. 6: Compact graph of the terminated SC TC receiver

- We have the same definitions for $I_e^k(i^-)$ and $I_a^k(i^-)$ with respect to the $\mathcal{O}_i^{-1}$ and $\mathcal{M}_{i-k}^{-1}$.

For the SC-TC, we perform all demappers updates and all outer decoders updates of each iteration in parallel as for the flooding scheduling used in standard belief propagation algorithm [12]. Using the fact that b_k represent proportions according to Eq. (1), the differences here with the uncoupled TC are the mixtures and the boundary conditions as follows:

- $I_e^k(i^+) = I_e(\mathcal{I}_i).b_k$ and $I_a(\mathcal{I}_i) = \sum I_a^k(i^+).b_k$
- $I_e^k(i^-) = I_e(\mathcal{O}_i).b_k$ and $I_a(\mathcal{O}_i) = \sum I_a^k(i^-).b_k$
- The *a priori* MIs coming from the added boundary nodes are equal to 1.

The threshold of the SC-TC is then defined as the lowest E_b/N_0 such as $I_{ap}(\mathcal{O}_i) \to 1, \forall i$.

Note that the obtained SC-EXIT chart can no more be interpreted graphically as in [14, Fig. 6], but are rather thought as a kind of Protograph EXIT (P-EXIT) chart [13], where the variable and check nodes are generalized and where the (m_s+1) incident edges are weighted by $\{b_k\}_k$.

C. Minimizing the number of iterations

The SC-EXIT chart analysis provides the asymptotic performance of an iterative scheme given a large number of iterations and a large codeword length. We can then apply classical non linear optimization methods to design coupling matrices such as [20]. When performing this optimization, we have observed that there exit several coupling matrices enabling to operate to the best achievable threshold (up to a given numerical precision). Among them, we have also observed that the convergence rate to this threshold was very different from one matrix to another. Therefore, an interesting additional criterion to consider when designing real systems is the convergence rate. In this section, we provide a framework that allows improving the convergence rate of SC-TC without altering

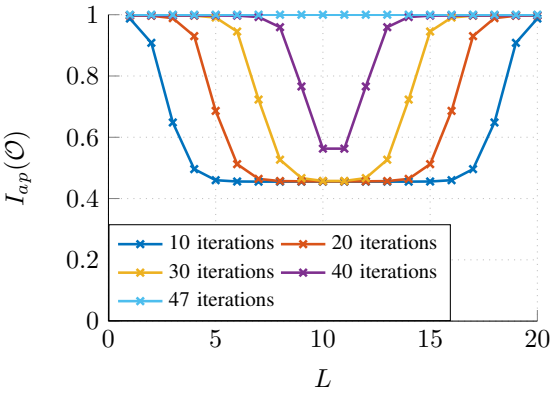

Fig. 7: Convergence of SC FTN at $E_s/N_0 = 5$dB.

the threshold or increasing the syndrome former memory m_s. To this aim, we consider the following procedure:

1) Pick an adequate initial coupling matrix B_0;
2) Evaluate the threshold of the corresponding SC-TC;
3) Find the optimal coupling B_{opt} such as:
   - The SC-TC converges at same threshold.
   - The number of iterations before convergence is minimal

Several trials showed that coupling with the uniform matrix B_0 (*ie.* all uniformly distributed non null entries b_k) is a good representative of the SC-TC ensemble defined by a fixed m_s, a fixed L and all possible Bs. Concerning the computation of the threshold in step 2, it can be estimated using the interval halving method. However, for step 3, two strategies can be adopted:

1) Search over a set of the form (with $N \in \mathbb{N}$): $\left\{\{b_k\}_k | \sum b_k = 1 \text{ and } b_k \in \{\frac{a}{N} | a \in [\![0, N]\!]\}\right\}$.
2) Since B belongs to a continuous space, we can perform the differential evolution algorithm [20].

The feasible set can be extremely reduced. Actually, due to the symmetry of the graph Fig. 5, both coupling matrices $B_1 = \{b_k\}_k$ and $B_1 = \{b_{m_s-k}\}_k$ lead to the same performance. Furthermore, the dimension of the problem can be reduced by replacing the equality constraint in Eq. (1) by the polytope:

$$\sum_{i=0}^{m_s-1} b_i \leq 1 \tag{3}$$

and deduce, at the end, $b_{m_s} = 1 - \sum_{i=0}^{m_s-1} b_i$.

NB: If B were an integer-valued vector, only the first strategy is possible and the optimization becomes infeasible especially for targeted values of n (asymptotic length) and m_s. This is the rational behind the choice of Eq. (1).

IV. Applications

A. Faster-Than-Nyquist based BICM

As a first application, we propose to illustrate an advanced BICM scheme based using a Faster-Than-Nyquist (FTN) waveform as a modulation device. This leads to a kind of bit interleaved coded modulation with memory that is efficiently decoded using iterative decoding. In this paper, we consider the circular FTN waveform as presented in [21]. Considering a root raised cosine (RRC) shaping filter with roll-off β and symbol period T. The

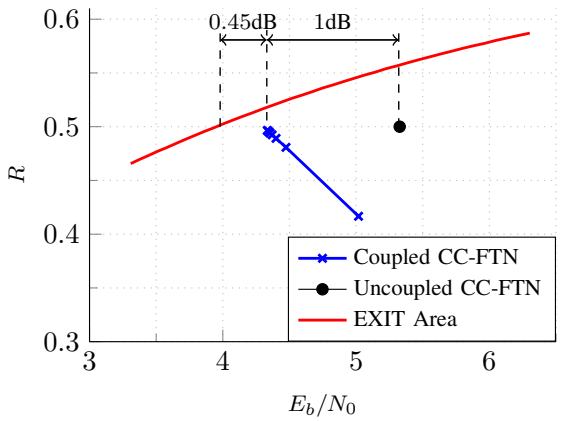

Fig. 8: Threshold of coupled and uncoupled proposed FTN scheme. Comparison to the Area under the EXIT is also depicted. $B = [\frac{1}{2}, \frac{1}{2}]$

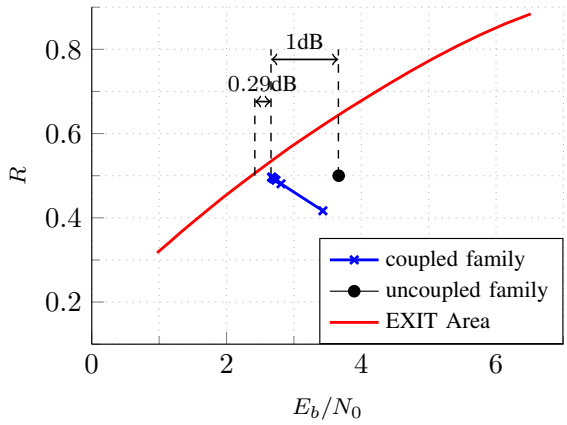

Fig. 9: Threshold of coupled and uncoupled proposed 16-QAM scheme. Comparison to the Area under the EXIT is also depicted. $B = [\frac{1}{2}, \frac{1}{2}]$

FTN symbol period is $T_s = \tau T$ where $\tau \in]0, 1]$ leads to an overall spectral efficiency of

$$\eta = \frac{R_L \log_2(M)}{\tau(1+\beta)} \ (bits/s/Hz).$$

Each coded and interleaved block $\mathbf{v}$ is modulated into $P = \left\lceil \frac{n}{\log_2(M)} \right\rceil$ symbols from the M-ary alphabet $\mathcal{M}$. Let $\mathbf{a} = [x_0, x_1, \dots x_{P-1}]$, the circular FTN waveform is obtained by circularly filtering these P symbols as follows:

$$x(t) = \sum_{p=0}^{P-1} x_p h_T(t - pT_s) w_T(t) \tag{4}$$

where $h_T(t) = \sum_{l=-\infty}^{\infty} h(t - lT)$ is the circular shaping filter and $w_T(t)$ is a window of length $T = PT_s$. At the receiver, a low complexity SISO equalizer for mitigating the Inter-Symbol Interference (ISI) introduced by FTN is considered as given in [21]. This is mainly based on a frequency domain fractionally spaced Linear Minimum Mean Square Error (L-MMSE) soft interference canceler (see [21] for more details).

1) Coupling gain: Figure 7 depicts the evolution of the *a posteriori* MI through iterations of the spatially-coupled serially concatenated scheme CC+FTN at $E_s/N_0 = 5$dB. The threshold of the uncoupled system is $E_s/N_0 = 5.32$dB. As expected, the known bits at the boundaries help propagate a coupling gain (also referred in the literature as the *wave effect*). Therefore, even if the E_s/N_0 is bellow the threshold of the uncoupled system, all stages converge after 47 iterations. In the meanwhile, the intermediate VNs behave as in the uncoupled system.

2) Threshold: In Fig. 8, we plot the threshold *vs* the rate[4] of the SC-TC FTN. For comparison, we included the uncoupled TC FTN and the threshold bound $\mathcal{A}^*$ given by the Area theorem [14]. As depicted, the coupling gain is of 1dB in comparison to the uncoupled system and is at just 0.45dB from $\mathcal{A}^*$. As L increases (here up to 145), we see that the spatially-coupled system saturates to a value very close to $\mathcal{A}^*$. This gap can be made smaller by considering larger L and a very big number of iterations.

3) Coupling optimization: With different syndrome former memories m_s and the best coupling matrices B, we observed that thresholds remain almost the same. Consequently and in order to simplify our analysis, we focus here only on the number of iterations before convergence. After running our optimization procedure, we observe that for our SC-CC FTN scheme, a coupling matrix of the form:

$$B_{\text{opt}} = [\frac{1}{2}, \quad (m_s - 1)\text{“0”s}, \quad \frac{1}{2}] \tag{5}$$

is the optimal form that minimizes the number of iterations without degrading the threshold. Figure 10 depicts the number of iterations for the *uniform* and the optimized B_{opt} coupling matrices. By changing the coupling matrix, we are able to converge 1.7, 2.13, 2.1, 2.6 and 3 times faster when m_s equals 2, 3, 4, 5 and 6 respectively at $L = 145$. For space issues, we choose to plot the results only for m_s equals 2, 3 and 6. On the other hand, observe that, with larger m_s, the convergence rate is faster. However, this comes at the expense of higher rate loss because a larger amount of known bits (black nodes) are introduced.

B. Linear modulation

Let us consider now the same systematic $[5, 7]$ outer code concatenated with a rate-1 accumulator of transfer function $1/(1+D)$. We choose 16-QAM modulations. In order to avoid a doubly-iterative system, we consider Gray mapping since its Exit chart is quasi flat. The obtained results are plotted in Figs. 9 and 11. One can see that the spatial coupling allows to gain 1dB in comparison to the uncoupled family and that we are at only 0.29dB from the threshold given by the area theorem.

When we optimize the coupling, the coupling matrix has no more the form in Eq. (5). The obtained coupling matrices are given in Fig. 11. Thanks to the coupling optimization, we are able to reduce the number of iterations by 1%, 22.3% and 20.8% when m_s equals 1, 2 and 3 respectively. On the other hand, when $m_s = 2$, observe that the convergence needs more iterations in comparison to $m_s = 1$: This is due to the fact that, by optimizing the coupling matrix, we are slightly improving the threshold in this case, but at the expense of more iterations.

V. Conclusion

In this paper, we presented a general framework of serially concatenated SC-TC. We showed the analogy with

[4]In order to obtain the spectral efficiency in (bits/s/Hz) in Fig. 8, multiply R by $log_2(M)/\eta$ where η is the occupied bandwidth.

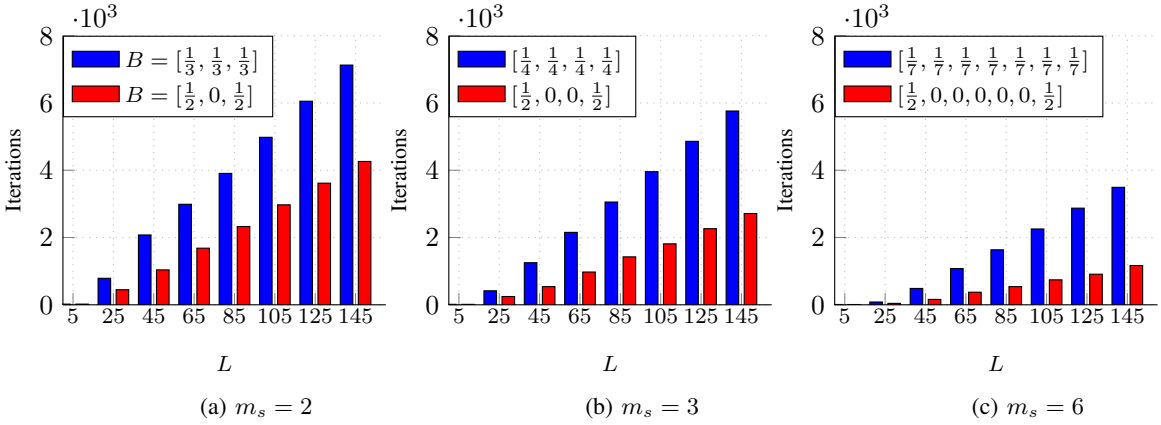

(a) $m_s = 2$ (b) $m_s = 3$ (c) $m_s = 6$

Fig. 10: Iterations before convergence of different syndrome former memories at the threshold given in Fig. 8

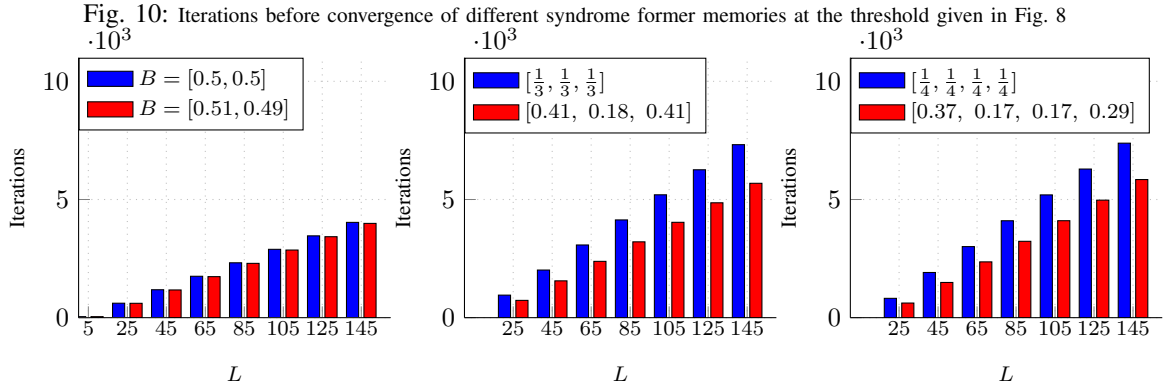

(a) $m_s = 1$ (b) $m_s = 2$ (c) $m_s = 3$

Fig. 11: Iterations before convergence of different syndrome former memories at the threshold given in Fig. 9

spatially-coupled protographs and described the SC-EXIT chart analysis. We optimized the coupling matrix and designed couplings with faster convergence rates. From the obtained results, we conjectured that the SC TC scheme saturates to a value very close (lower bounded) by the Area theorem. Future work will investigate other channels and study the performance of window decoding.

REFERENCES

[1] A. Jimenez Felstrom and K. S. Zigangirov, "Time-varying periodic convolutional codes with low-density parity-check matrix," *IEEE Trans. Inf. Theory*, vol. 45, no. 6, pp. 2181–2191, 1999.

[2] S. Kudekar, T. J. Richardson, and R. L. Urbanke, "Threshold saturation via spatial coupling: Why convolutional ldpc ensembles perform so well over the bec," *IEEE Trans. Inf. Theory*, vol. 57, no. 2, pp. 803–834, 2011.

[3] S. Kumar, A. J. Young, N. Macris, and H. D. Pfister, "Threshold saturation for spatially coupled ldpc and ldgm codes on bms channels," *IEEE Trans. on Inf. Theory*, vol. 60, no. 12, pp. 7389–7415, 2014.

[4] P. S. Nguyen, A. Yedla, H. D. Pfister, and K. R. Narayanan, "Spatially-coupled codes and threshold saturation on intersymbol-interference channels," *arXiv preprint arXiv:1107.3253*, 2011.

[5] A. E. Pusane, R. Smarandache, P. O. Vontobel, and D. J. Costello, "Deriving good ldpc convolutional codes from ldpc block codes," *IEEE Trans. on Inf. Theory*, vol. 57, no. 2, pp. 835–857, 2011.

[6] D. G. Mitchell, M. Lentmaier, and D. J. Costello Jr, "Spatially coupled ldpc codes constructed from protographs," *arXiv preprint arXiv:1407.5366*, 2014.

[7] S. Moloudi, M. Lentmaier, and A. G. i Amat, "Spatially coupled turbo codes," in *8th International Symposium on Turbo Codes and Iterative Information Processing (ISTC), 2014*. IEEE, 2014, pp. 82–86.

[8] S. Moloudi, M. Lentmaier *et al.*, "Spatially coupled turbo-like codes," *arXiv preprint arXiv:1604.07315*, 2016.

[9] D. J. Costello, M. Lentmaier, and D. G. Mitchell, "New perspectives on braided convolutional codes," in *9th International Symposium on Turbo Codes and Iterative Information Processing (ISTC), 2016*. IEEE, 2016, pp. 400–405.

[10] W. Zhang, M. Lentmaier, K. S. Zigangirov, and D. J. Costello Jr, "Braided convolutional codes: a new class of turbo-like codes," *IEEE Trans. on Inf. Theory*, vol. 56, no. 1, pp. 316–331, 2010.

[11] S. Moloudi, M. Lentmaier *et al.*, "Finite length weight enumerator analysis of braided convolutional codes," *arXiv preprint arXiv:1608.02355*, 2016.

[12] W. Ryan and S. Lin, *Channel codes: classical and modern*. Cambridge University Press, 2009.

[13] G. Liva and M. Chiani, "Protograph ldpc codes design based on exit analysis," in *IEEE Global Telecommunications Conference, 2007. GLOBECOM'07*, 2007, pp. 3250–3254.

[14] J. Hagenauer, "The exit chart-introduction to extrinsic information transfer in iterative processing," in *Proc. 12th European Signal Processing Conference (EUSIPCO)*, 2004, pp. 1541–1548.

[15] C. Berrou and A. Glavieux, "Near optimum error correcting coding and decoding: Turbo-codes," *IEEE Trans. Commun.*, vol. 44, no. 10, pp. 1261–1271, 1996.

[16] A. G. i Fàbregas, A. Martinez, G. Caire *et al.*, "Bit-interleaved coded modulation," *Foundations and Trends® in Communications and Information Theory*, vol. 5, no. 1–2, pp. 1–153, 2008.

[17] L. Bahl, J. Cocke, F. Jelinek, and J. Raviv, "Optimal decoding of linear codes for minimizing symbol error rate (corresp.)," *IEEE Trans. Inf. Theory*, vol. 20, pp. 284–287, 1974.

[18] A. G. i Amat, S. Moloudi, and M. Lentmaier, "Spatially coupled turbo codes: Principles and finite length performance," in *11th International Symposium on Wireless Communications Systems (ISWCS), 2014*. IEEE, 2014, pp. 883–887.

[19] S. ten Brink, "Convergence behavior of iteratively decoded parallel concatenated codes," *IEEE Trans. Commun.*, vol. 49, no. 10, pp. 1727–1737, 2001.

[20] R. Storn and K. Price, "Differential evolution–a simple and efficient heuristic for global optimization over continuous spaces," *Journal of global optimization*, vol. 11, no. 4, pp. 341–359, 1997.

[21] R. Tajan, C. Poulliat, and M. L. Boucheret, "Circular faster than nyquist: Transmitter and iterative receiver design," in *International Symposium on Turbo Codes and Iterative Information Processing (ISTC)*, Sept 2016, pp. 241–245.